

FEDSM-ICNMM2010-' \$+- '

AIR FLOW SIMULATION IN A DIESEL ENGINE

Joaquín Fernández Alfonso Marcos

Universidad de Extremadura. Departamento de IMEM
Badajoz, Extremadura, Spain

Raúl Barrio Eduardo Blanco

Universidad de Oviedo. Departamento de Energía
Gijón, Asturias, Spain

Alejandro Castilla

Deutz-Diter S.A.
Zafra, Extremadura, Spain

ABSTRACT

The intake manifold of a Diesel engine is of significant importance. Several modifications are usually carried out in this system to increase the power generated without modifying the general design of the engine. This work presents a numerical and experimental investigation on the air flow in a commercial Diesel engine. The air average mass flow through the intake manifold was obtained experimentally for the D909 Deutz-Diter Diesel engine. Additionally, a numerical model was created for the test engine. The model reproduces the operating and boundary conditions of the flow and integrates the equations that describe the motion of the fluid. The average mass flow through the engine was obtained from the model and compared with the experimental measurements. The model was used subsequently to investigate the air flow within the engine.

INTRODUCTION

In a Diesel engine, only air is initially introduced in the combustion chamber by the negative pressure difference induced by the displacement of the piston. The fuel is injected directly into the chamber just before the combustion process is started. The loading is regulated by varying the amount of fuel injected; in contrast, the air mass flow does not change significantly for a specific speed of rotation. The intake manifold is of great importance in an internal combustion engine because this system has a significant influence on the power generated, fuel consumption, emission of pollutants, etc. For this reason, it is not an unusual practice to modify the geometry of the intake manifold in order to increase the generated power without proposing a new design for the engine.

The power generated is fairly proportional to the air mass flow [1, 2]. As a first approximation, operation under a stationary regime is considered to evaluate the dependence of

the air mass flow on the geometry of the inlet manifold [3]. With this approximation, air flows through the system for a fixed valve lift and the piston is eliminated. Suction is then produced by a fan located at the bottom of the cylinder. The fan generates a pressure difference between the intake manifold and the cylinder. This type of experimental set-up is used to obtain the dependence between the air mass flow and the valve lift for a fixed pressure difference. However, this stationary approximation neglects both the dynamic effects of the flow and the influence of combustion.

In general, the air flow in a Diesel engine is three-dimensional, including secondary flows, unsteady phenomena, etc. [4]. The numerical simulation of the flow is not straightforward due to the classical difficulties found when using Computational Fluid Dynamics (CFD) software: turbulence, flow separation, etc [5]. There are also other specific problems that deal with the complexity of the geometry, which requires a large number of computational cells, or with the displacement of the piston, which causes a temporal variation in the volume of the combustion chamber. In spite of these difficulties, CFD software has proven to be a useful tool for the design and prediction of the performance of internal combustion engines.

This paper presents numerical and experimental work on the air flow in a commercial Diesel engine. A numerical model for the engine was first created and subsequently simulated with the code Fluent. This code uses the finite volume method to solve the Navier-Stokes equations. The simulations were carried out taking into account the real 3D-geometry of the motor and the unsteady nature of the flow. The predictions from the model were validated by a series of laboratory tests. The model was finally used to predict the air flow distribution in the engine.

NUMERICAL MODEL

The test engine is the model D909 manufactured by Deutz-Diter (see Fig. 1). This is a one-cylinder four-stroke engine with natural suction, direct injection, and air-refrigerated. The engine has a cylinder capacity of 0.709 l, a maximum power output of 11 kW at 3000 rpm and a maximum torque of 38.5 N·m at 2000 rpm.



Fig. 1 The D909 Deutz-Diter Diesel engine.

The intake manifold comprises a tube, a conduit, eight rings, and a valve. The cylinder is not a part of this system strictly speaking, but it has a significant influence on the incoming and outgoing flux of gases in the engine. The shape of the conduit helps vorticity development, so that the mixing process with the fuel is improved. The connection of the inlet manifold and the cylinder through the rings is crucial for the incoming of the amount of air desired. Fig. 2 shows the numerical model of the intake and exhaust manifolds and of the cylinder (a); also, a detail of the surface mesh of the cylinder is presented (b).

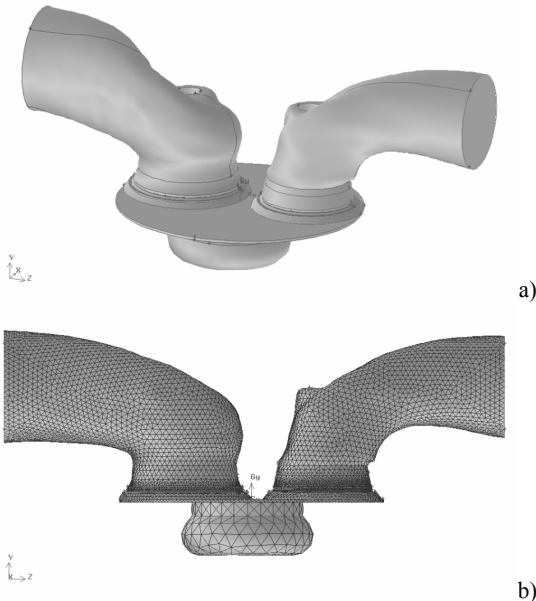


Fig. 2 Numerical model of the engine (a) and detail of the surface mesh of the intake and exhaust manifolds (b).

The mesh was both structured and unstructured. The stationary zones of the domain were meshed using unstructured cells. In contrast, the regions of the geometry containing boundaries in relative motion (this is the case of the intake and exhaust valves and the piston) were specially meshed. The zone of fluid that surrounds the valves inside the intake and exhaust manifolds contains structured cells; more cell layers are added as the valves progress in their motion. Inside the cylinder there are two simultaneous movements: the one of the valves and that of the cylinder. The mesh is unstructured near the valves and, in addition, a subsequent re-meshing allows their motion.

Once valve lift distance is reached, structured cell layers are added as the piston progresses. This can be observed in Fig. 3, which shows an image of the mesh for two relative positions of the piston. The number of cells used to start the simulations (piston at the top position) was about $2.5 \cdot 10^5$, though other meshes of different size were generated to investigate the dependence of the numerical predictions, as will be explained. The maximum equiangle skew was restricted below 0.6 for 98% of the cells in the mesh.

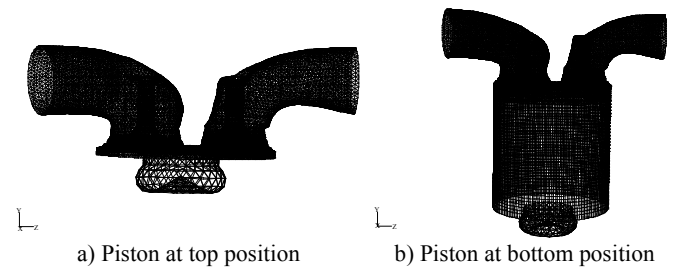


Fig. 3 Dynamic mesh of the cylinder for two positions of the piston.

The numerical simulations were performed with the code Fluent. This code is used to solve the full unsteady 3D Navier-Stokes equations by the finite volume method [6]. Turbulence was simulated with the realizable k -epsilon model together with logarithmic wall functions to resolve the flow variables in the boundary layer region. The time dependent term scheme was second order and implicit. The pressure-velocity coupling was established by means of the PISO algorithm with proximity correction. Second-order upwind discretizations were used for the convection terms and central difference discretizations were used for the diffusion terms.

The boundary condition imposed at the inlet of the domain was a zero gauge total pressure together with a temperature of 300 K and a turbulent intensity of 5%. The outlet boundary condition is a zero gauge pressure, a temperature of 300 K, and a turbulent intensity of 5%. A non-slip condition was imposed in the solid boundaries, supposed as adiabatic walls. The air was supposed as a perfect gas with constant specific heats at the very beginning of the simulations. As explained later, the dependence between the specific heats and temperature was also investigated using the equation:

$$C_p = 953.6 + 0.18182T \text{ [J/(kg K)]}. \quad (1)$$

The initial condition used to start the simulations was a zero velocity when the piston is at its bottom position. This allowed reaching a periodic regime yet at the end of the first simulation cycle. The simulations were carried out for two rotation speeds of the engine: 1700 and 3000 rpm. In both cases, the intake and exhaust valves opened at a crank angle of -18° and 484° respectively. The valves closed at 238° (intake) and 22° (exhaust). The time step size used in the unsteady calculations was $2.45 \cdot 10^{-5}$ s for the angular velocity of 1700 rpm and $1.39 \cdot 10^{-5}$ s for the 3000 rpm velocity. This is equivalent to an angle of rotation of the crank between two consecutive time steps of 0.25° . The re-meshing of the engine is related with the magnitude of the time step and also with the rotation speed. The engine completes a simulation cycle every 2880 time steps. Several tests were performed using half the time step size imposed in the final calculations and no significant differences were found. The number of iterations in each time step was adjusted to reduce the magnitude of the residuals below an acceptable level. Fig. 4 shows an example of convergence history. As observed, the residuals converge quickly and reach negligible magnitudes.

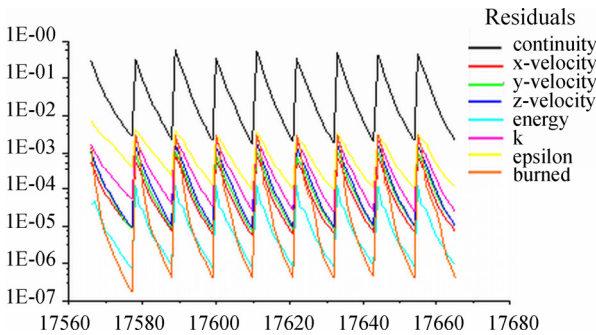


Fig. 4 Example of convergence history.

The dependence between the numerical predictions and the mesh size was investigated by varying the number of cells in the mesh. The obtained results of the average mass flow for a valve lift of 3 mm are compared in Fig. 5 with the data collected from an experimental arrangement (see following section). The x -axis in the figure shows the mesh size (as observed, four test meshes were created) and the y -axis presents the relative error between the numerical predictions and the experimental measurements. It is observed in Fig. 5 that the general performance of the engine does not change significantly (only excluding the lower mesh size) even when doubling the number of cells.

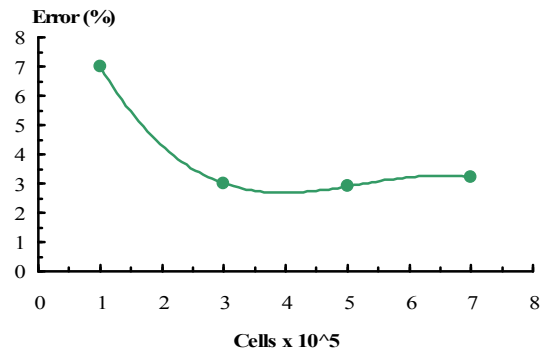


Fig. 5 Grid dependence analysis of the numerical predictions.

EXPERIMENTAL TESTS AND VALIDATION

The experimental tests were carried out in the standard test rig by Deutz-Diter shown in Fig. 6. During the tests, the rotational velocity was fixed and the air inside the motor followed the Diesel cycle, only excluding the combustion process. The air comes into the cylinder through the intake valve and leaves the motor through the exhaust valve. Therefore, combustion processes and transient phenomena associated to temporal variations of other variables are not taken into consideration. The flow can be considered as adiabatic.



Fig. 6 General layout of the test rig.

Table 1 and Table 2 show a comparison between the numerical predictions and the experimental results of the average air mass flow and the maximum pressure in the cylinder (estimated uncertainty $\sim 4\%$). As observed, the prediction of the average mass flow is in quite good agreement with the experimental data, showing maximum relative errors of about 3%. However, larger differences are found for the pressure in the cylinder. These differences can be attributable, to some extent, to the decrease of the mass flow sucked in due to the heating of the incoming air that is in contact with the cylinder walls, and to the losses through the gap between the piston and the cylinder walls (neglected in the numerical model).

Table 1. Air average mass flow predicted and measured [kg/s].

	1700 rpm		3000 rpm
	C_p constant	C_p variable	C_p constant
Tests	$1.069 \cdot 10^{-2}$		$1.922 \cdot 10^{-2}$
Predictions	$1.071 \cdot 10^{-2}$	$1.079 \cdot 10^{-2}$	$1.858 \cdot 10^{-2}$
Error (%)	0.10	0.88	-3.33

Table 2. Pressure in the cylinder predicted and measured [Pa].

	1700 rpm		3000 rpm
	C_p constant	C_p variable	C_p constant
Tests	5357000		6062700
Predictions	6672756	6434011	7214953
Error (%)	24.5	20.1	19.0

The maximum pressure in the cylinder as a function of the crank angle is presented in Fig. 7 for a speed of rotation of 1700 rpm. The numerical predictions shown were obtained for both a constant and variable C_p . Correspondence between crank angle values and motor valves position is:

- 18° intake valve opening, simulation starts
- 0° top dead centers
- 180° bottom dead centers
- 238° close of intake valve
- 360° top dead centers, end of compression
- 484° exhaust valve opening
- 540° bottom dead centers
- 720° top dead centers
- 22° close of exhaust valve

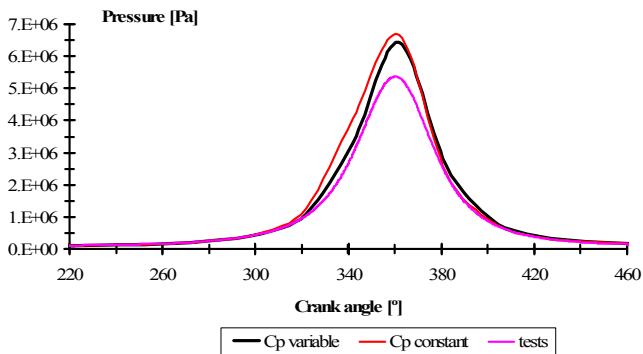


Fig. 7 Maximum pressure in the cylinder for a speed of rotation of 1700 rpm. Test results and numerical predictions.

Fig. 8 shows the temperature evolution as a function of the crank angle for a speed of rotation of 1700 rpm. Additionally, the evolution of the temperature obtained from the adiabatic equation for constant specific heats is also shown [7]:

$$T_{adi} = T_0 \left(\frac{p}{p_0} \right)^{\gamma-1/\gamma} = T_0 \left(\frac{p}{p_0} \right)^{1-C_p/C_v} \quad (2)$$

using the pressures obtained from the simulations. The differences found between the temperatures obtained from the simulations using a constant specific heat and the adiabatic

temperature can be attributable to the viscous heating in the cylinder. Larger differences were observed for the adiabatic law at 3000 rpm; this can be due to an increase of viscous dissipation with increasing rotational speeds.

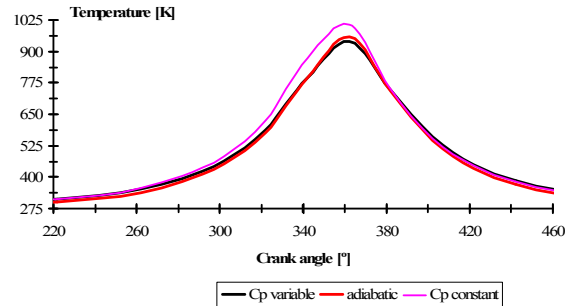
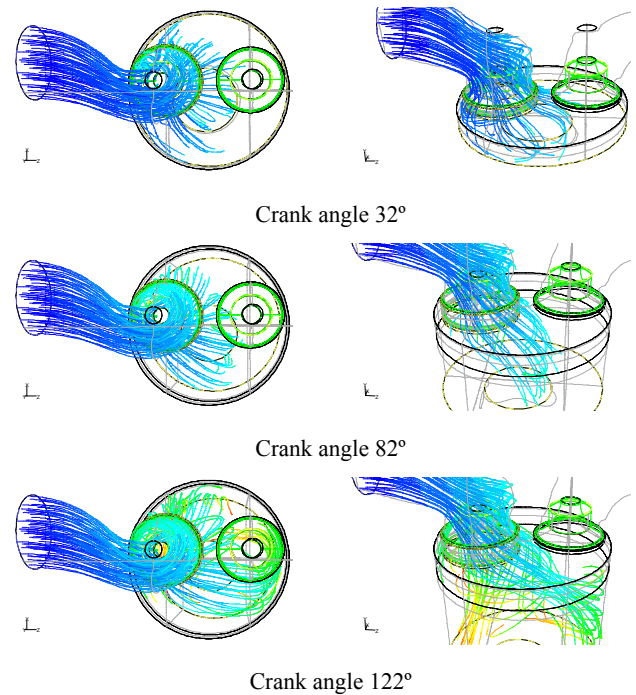


Fig. 8 Predicted and adiabatic temperature for a speed of rotation of 1700 rpm.

NUMERICAL RESULTS

The numerical simulations were carried out for a speed of rotation of 1700 rpm (C_p constant and variable) and 3000 rpm (C_p constant). Fig. 9 shows the traces of the fluid particles in the cylinder during a complete piston stroke for a speed of rotation of 1700 rpm. It can be observed that the air comes into the cylinder while rotating in a counter-clockwise direction induced by the intake manifold. This rotating motion is damped in the cylinder due to the effect of the friction with the lateral walls. The air progresses into the cylinder while moving near the walls.



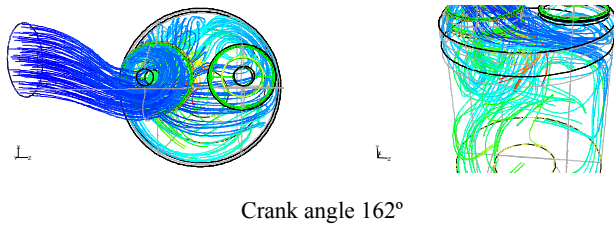


Fig. 9 Traces of air particles for several crank angles.

Fig. 10 shows the magnitude of angular momentum at 1700 rpm for C_p both constant and variable. It can be seen that the variation of the specific heat has little influence in the angular momentum.

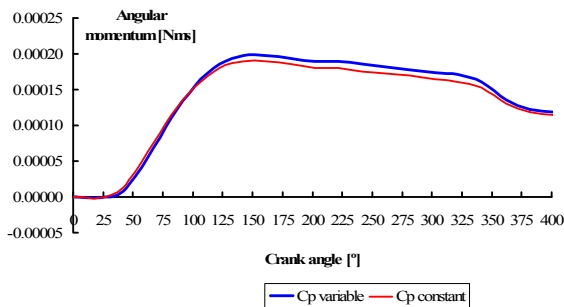


Fig. 10 Angular momentum for C_p constant and variable (rotation speed = 1700 rpm).

Fig. 11 presents the surface distribution of angular momentum when the piston is at its top position. The results shown were obtained in a plane perpendicular to the direction of motion of the piston. It is observed that the higher magnitudes of angular momentum are predicted near the right wall of the cylinder, where the tangential velocities are also high (according to Fig. 9). Obviously, the lower values of angular momentum are obtained near the cylinder axis.

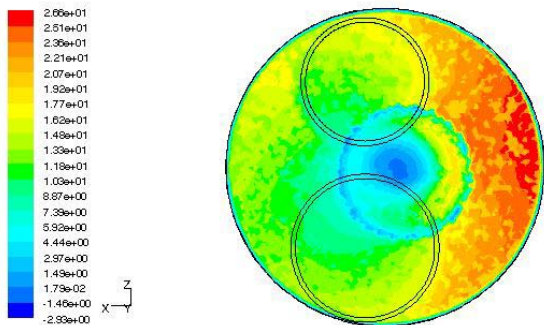


Fig. 11 Contours of angular momentum (Nms) at 1700 rpm (piston at top position).

The efficiency of the mixture process between the air and the fuel improves with increasing turbulence. The magnitude of turbulence is usually characterized by a parameter known as turbulent intensity, defined as follows:

$$I = \frac{\sqrt{2/3 k}}{v_{ref}}, \quad (3)$$

where k is the turbulent kinetic energy and v_{ref} is a reference velocity. Fig. 12 shows the contours of turbulent intensity with the piston at its top position and a reference velocity of 100 m/s. As observed, turbulence is more intense at the middle region of the cylinder.

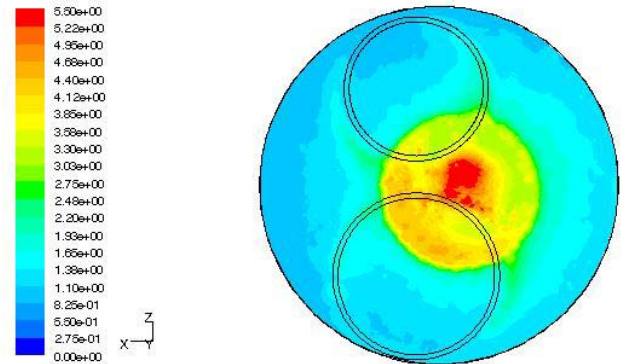
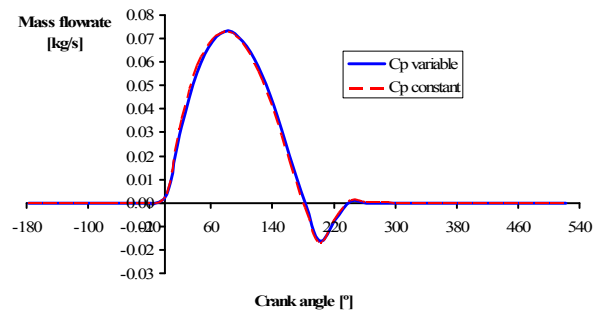
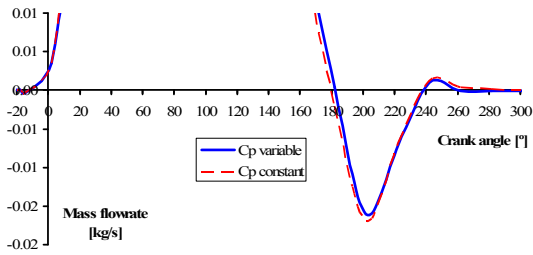


Fig. 12 Contours of turbulent intensity (%) obtained at 1700 rpm (piston at top position).

The instantaneous mass flow rate through the intake manifold during a complete stroke cycle is presented in Fig. 13. The results shown in the figure were obtained for a speed of rotation of 1700 rpm when considering the specific heat both constant and variable. Fig. 13 shows also a detail of the cycle period between the opening and closing of the valves. As observed, the obtained results do not change significantly if the correction for C_p (equation 1) is introduced. The opening of the intake valve before the piston reaches the top position hardly causes a backflow in the intake manifold. This is because the exhaust valve is also opened. In contrast, the delay in the closing of the intake valve (after the piston reaches its bottom position) causes a significant backflow, as can be appreciated in Fig. 13b. Just after this point, the instantaneous mass flow rate turns to negative values, reaching a minimum at 200° and then equaling zero at 238°, when the valve closes.



a)



b)

Fig. 13 Instantaneous mass flow rate (kg/s) at 1700 rpm (C_p constant and variable).

Fig. 14 shows the instantaneous mass flow rate for a speed of rotation of 3000 rpm. It is seen that the obtained results are similar to those presented in Fig. 13, except for when the piston is at its bottom position. In this case, the mass flow rate turns to negative values at a crank angle of 190°. It can be observed that the mass flow rate is proportional to the speed of rotation, thus indicating that the volumetric efficiency does not change significantly with rotation velocity.

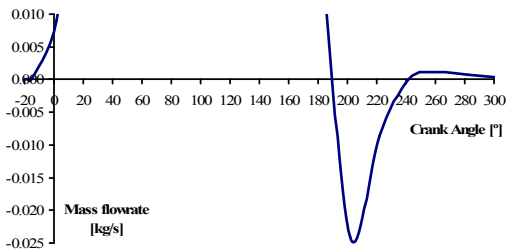
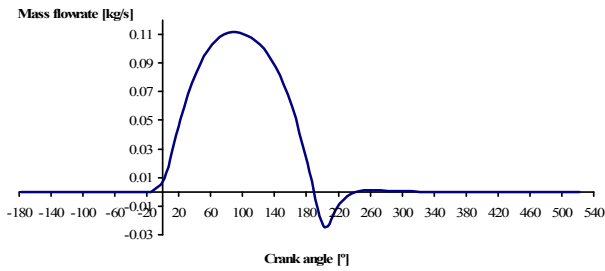


Fig. 14 Instantaneous mass flow rate (kg/s) at 3000 rpm (constant C_p)

Finally, Fig. 15 presents some contours of several variables obtained in a plane parallel to the direction of motion of the piston. In this case, the piston is located at its bottom position. The figure shows the filling process of the cylinder with the incoming air.

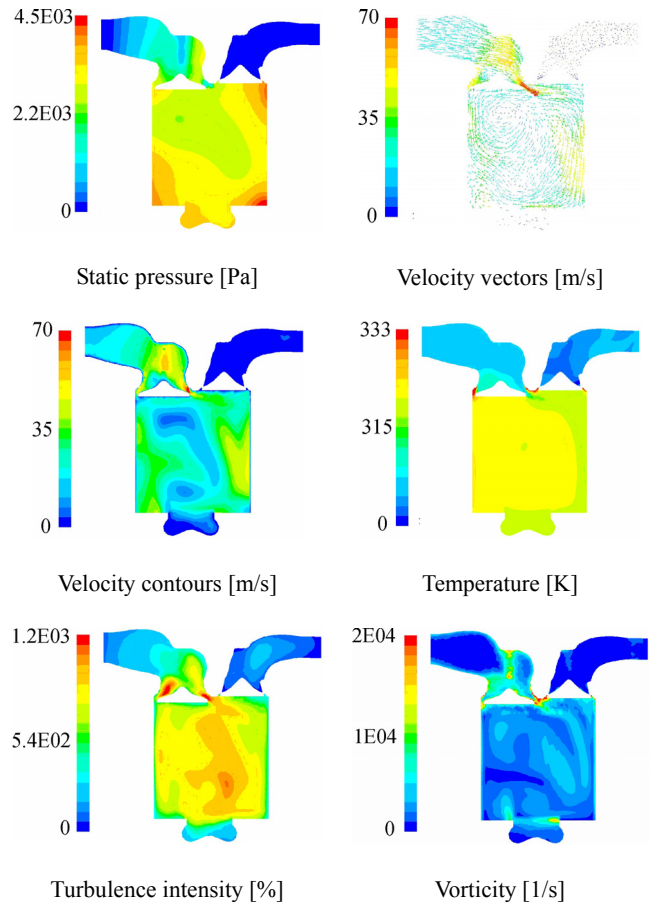


Fig. 15 Contours of several variables when the piston is at the bottom section of the cylinder.

CONCLUSIONS

A numerical simulation of the air flow in a Diesel engine was presented. The simulations were carried out for 3D unsteady flow using the code Fluent. The mesh of the cylinder and of the inlet and exhaust valves was dynamic, that is, successive mesh layers were generated to allow the motion of both the valves and the piston. The numerical model was validated using experimental data obtained in a test rig at laboratory. It was observed that the numerical predictions were in good agreement with the experiments, showing relative errors lower than 3% for the air average mass flow. The model was finally used to investigate the air flow distribution within the engine and the temporal evolution of some significant variables. As a final conclusion, it can be said that the reported procedure (numerical simulation of the unsteady flow with a commercial code) provides satisfactory results that can be used to design new engine prototypes.

NOMENCLATURE

C_p, C_v	specific heat at constant pressure or volume [J/(kgK)]
I	turbulent intensity [%]
k	turbulent kinetic energy [m^2/s^2]
p	pressure [Pa]
T, T_{adi}	temperature, adiabatic temperature [K]
v_{ref}	reference velocity [m/s]
γ	$= C_p/C_v$ specific heat ratio [-]

ACKNOWLEDGMENTS

The authors gratefully acknowledge the financial support provided by Consejería de Educación, Ciencia y Tecnología de la Junta de Extremadura under project 2PR04A073.

REFERENCES

- [1] Della Volpe, R., 2001, *Impianti Motori per la Propulsione Navale*, Liguori Editori, Italy.
- [2] Garro, A., 1992, *Progettazione Strutturale del Motore*, Levrotto & Bella, Italy.
- [3] Genta, G., 2000, *Meccanica dell'Autoveicolo*, Levrotto & Bella, Italy.
- [4] Batchelor, G. K., 2000, *An Introduction to Fluid Dynamics*, Cambridge University Press, London.
- [5] Ferziger, J. H., Peric, M., 1996, *Computational Methods for Fluid Dynamics*, Springer, New York.
- [6] Versteeg, H. K., Malalasekera, W., 1995, *An Introduction to Computational Fluid Dynamics. The Finite Volume Method*, Longman Scientific and Technical, England.
- [7] White, F. M., 2004, *Fluid Mechanics*, McGraw-Hill, London.